Intracellular Features Predicted by Extracellular Recordings in the Hippocampus In Vivo

DARRELL A. HENZE, ZSOLT BORHEGYI, JOZSEF CSICSVARI, AKIRA MAMIYA, KENNETH D. HARRIS, AND GYÖRGY BUZSÁKI
Center for Molecular and Behavioral Neuroscience, Rutgers, The State University of New Jersey, Newark, New Jersey 07102

Henze, Darrell A., Zsolt Borhegyi, Jozsef Csicsvari, Akira Mamiya, Kenneth D. Harris, and György Buzsáki. Intracellular features predicted by extracellular recordings in the hippocampus in vivo. *J Neurophysiol* 84: 390–400, 2000. Multichannel tetrode array recording in awake behaving animals provides a powerful method to record the activity of large numbers of neurons. The power of this method could be extended if further information concerning the intracellular state of the neurons could be extracted from the extracellularly recorded signals. Toward this end, we have simultaneously recorded intracellular and extracellular signals from hippocampal CA1 pyramidal cells and interneurons in the anesthetized rat. We found that several intracellular parameters can be deduced from extracellular spike waveforms. The width of the intracellular action potential is defined precisely by distinct points on the extracellular spike. Amplitude changes of the intracellular action potential are reflected by changes in the amplitude of the initial negative phase of the extracellular spike, and these amplitude changes are dependent on the state of the network. In addition, intracellular recordings from dendrites with simultaneous extracellular recordings from the soma indicate that, on average, action potentials are initiated in the perisomatic region and propagate to the dendrites at 1.68 m/s. Finally we determined that a tetrode in hippocampal area CA1 theoretically should be able to record electrical signals from ~1,000 neurons. Of these, 60–100 neurons should generate spikes of sufficient amplitude to be detectable from the noise and to allow for their separation using current spatial clustering methods. This theoretical maximum is in contrast to the approximately six units that are usually detected per tetrode. From this, we conclude that a large percentage of hippocampal CA1 pyramidal cells are silent in any given behavioral condition.

INTRODUCTION

The study of how the activity of single neurons contribute to network computations requires the ability to record the simultaneous activity of large numbers of neurons. The use of multichannel extracellular recording techniques has improved single-unit sorting by taking advantage of the temporal coherence of spikes from closely-spaced recording sites (Buzsaki and Kandel 1998; Drake et al. 1988; McNaughton et al. 1983; Recce and O'Keefe 1989; Wilson and McNaughton 1993). An important outstanding issue is what is the maximum number of simultaneously recordable neurons that can be achieved using extracellular recording techniques. The maximum number of detectable cells is expected to vary across brain regions de-

pending on variables such as neuronal density and activity. Here we focus our attention on unit detection in the rat hippocampal area CA1.

Extracellular recording methods traditionally provide information only on whether a neuron fires a spike or not. To obtain information about subthreshold variations in neuronal membrane potential, it is necessary to use intracellular recording methods. In addition, intracellular recording has the added advantage that it allows subsequent morphological identification of the recorded neuron. However, intracellular recordings typically are obtained from one cell at a time under nonphysiological conditions, e.g., in tissue slices and anesthetized brains. Since the extracellularly recorded spikes arise due to transmembrane currents and concurrent changes in intracellular membrane potential, it should be possible to obtain more detailed information about intracellular changes from close examination of the extracellular spikes. However, this requires a better understanding of the relationship between an intracellular action potential and the extracellular spike.

The present experiments provide important information about the sensitivity of the tetrode recording method and investigate the relationship between intracellular action potentials and extracellular spikes. Our investigations ask the following questions: what is the precise temporal relationship between the intracellularly recorded somatic and dendritic action potential and its extracellularly recorded counterpart? Does variation in the intracellular action potential contribute to amplitude and shape variability of extracellular spikes? How close does a neuron have to be to a tetrode to be detected and subsequently isolated during analysis?

METHODS

Simultaneous intracellular-extracellular recording in anesthetized rats

Thirty rats (350–450 g) of the Sprague-Dawley strain (Hilltop Labs, Scottsdale, PA) were anesthetized with urethan (1.5 g/kg; Sigma) and placed in a stereotaxic apparatus. The body temperature of the rat was kept constant by a small animal thermoregulation device. The scalp was removed, and a small (1.2 × 1.2 mm) bone window was drilled above the hippocampus (centered at AP = −3.5 and L = 2.5 mm from bregma) for extra- and intracellular recordings. A pair of

stimulating electrodes (100 μm each, with 0.5-mm tip separation) were inserted into the left fimbria-fornix (AP = -1.3, L = 1.0, V = 3.95) to stimulate the commissural inputs. Extracellular and intracellular electrodes were mounted on two separate manipulators on opposite sides of a Kopf stereotaxic apparatus. The horizontal axes of the two manipulators were parallel. The manipulator of the extracellular electrode was mounted at a 10° angle from vertical to permit the subsequent placement of the intracellular electrode. The optimal distance between the electrodes at the brain surface to cause the tips to arrive at the same point at the level of the hippocampus (2 mm deep) was calculated to be ~370 μm. The extracellular electrode was lowered into the cell body layer of CA1 by monitoring for the presence of unit activity and evoked field potentials. Once the intracellular and extracellular electrode tips were placed in the brain, the bone window was covered by a mixture of paraffin (50%) and paraffin oil (50%) to prevent drying of the brain and decrease pulsation. The intracellular micropipette was then advanced into the region near the extracellular electrode, and an intracellular recording from a CA1 pyramidal cell was obtained. If no extracellular and intracellular pairs were encountered after advancing the micropipette through the CA1 pyramidal layer and stratum radiatum, the intracellular electrode was withdrawn, and a new intracellular electrode track was made from the cortical surface.

Detection of intracellular action potentials and extracellular spikes

Intracellular action potentials were detected by examining the first derivative of the membrane potential for peaks. Once a peak was detected in the first derivative, the actual peak of the AP was determined from the point where the first derivative crossed back through zero. The extracellular spikes were extracted based on the occurrence of the intracellular action potential.

The extracellular "tetrodes" (Recce and O'Keefe 1989) consisted four 13-μm polyimide-coated nichrome wires (H. P. Reid, Palm Coast, FL) bound together by twisting them and then melting their insulation (Gray et al. 1995). In five rats, the extracellular electrode consisted of a single 60-μm wire. The extracellular signal was amplified 1,000–8,000 times using a DC amplifier and filtered at 1–3,000 Hz (Model-12, Grass Instruments, West Warwick, RI). The micropipettes for intracellular recordings were pulled from 2.0-mm capillary glass (World Precision Instruments, Sarasota, FL) and filled with 1 M potassium acetate (Fisher Scientific, Pittsburgh, PA). The electrode solution also contained 2% biocytin (Sigma, St. Louis, MO) for single-cell labeling of all recorded cells. In vivo electrode impedances were between 60 and 110 MΩ as measured by the bridge balance circuit of the amplifier (Axoclamp-2A, Axon Instruments, Foster City, CA). Once stable intracellular recordings were obtained (resting membrane potentials less than -55 mV), evoked and passive physiological properties of the cell were determined. All electrophysiological signals were digitized [sampled at 10, 20, 25, or 50 kHz at 12 or 16 bit resolution (R. C. Electronics, Santa Barbara, CA)] and stored on computer disk for later analysis.

Histological procedures

After the completion of the intracellular physiological data collection, biocytin was injected through a bridge circuit using 500-ms depolarizing pulses at 0.6–2 nA at 1 Hz for 10–60 min. Neuronal activity was followed throughout the procedure, and the current was reduced if the electrode was blocked and/or the condition of the neuron deteriorated. Two to 12 h after the injection, the animals were given an urethan overdose and then perfused intracardially with 100 ml physiological saline followed by 400 ml of 4% paraformaldehyde and 0.2% glutaraldehyde dissolved in phosphate buffered saline (pH = 7.2). The brains were then removed and stored in the fixative solution overnight. Sixty-micrometer-thick coronal sections were cut

and processed for biocytin labeling. The histological sections were also used to verify the position of the extracellular recording electrodes and the track made by the recording pipette. The orientation between the labeled neuron and the tip of the tetrode was reconstructed by tracing the neuron soma and the tetrode track using a drawing tube. The distance between the neuron and the electrode tip was measured from the traced image. If the tetrode tip was in a different section than the neuronal soma, the Pythagorean theorem was used to calculate the distance.

Extracellular recording in behaving animals

SURGERY AND RECORDING. The surgical procedures, electrode preparation, and implantation methods have been described in a previous study (Csicsvari et al. 1999a). The data from that previous study was re-examined for the analyses presented here. In short, 19 male rats were implanted with either wire "tetrodes" or silicon electrode arrays that were used for recording of neuronal activity. Silicon electrode arrays were fabricated using integrated circuit technology. The shanks of the silicon probes were separated by either 150 or 300 μm. Each shank contained four or six recording sites (9 $\times$ 12 μm platinum pads) with 25-μm vertical spacings (Ylinen et al. 1995). The electrodes are attached to a multidrive array, and the electrodes were slowly advanced until they reached the CA1 pyramidal layer. Two 50-μm single tungsten wires (with 2 mm of the insulation removed) were inserted into the cerebellum and served as ground and reference electrodes.

DATA PROCESSING. Electrical activity was recorded during sleep while the rat was in its home cage (Csicsvari et al. 1999a). After amplification (5,000–10,000 times) and band-pass filtering (1 Hz to 5 kHz; Model 12–64 channels; Grass Instruments), field potentials and extracellular spikes were recorded continuously and digitized (10–50 kHz at 12 or 16 bit resolution, R. C. Electronics) and stored on computer disk for later analysis. Recording sessions lasted from 15 to 50 min. The separation and analysis of the extracellular units was accomplished using standard cluster based separation methods detailed elsewhere (Csicsvari et al. 1999a).

RESULTS

Simultaneous extracellular and intracellular recordings were obtained from area CA1 of the dorsal hippocampus of anesthetized rats. In cases where the electrode placements were accurate, simultaneous spikes were observed in the extracellular and intracellular recordings as the intracellular electrode was advanced through the tissue and attempts were made to obtain stable intracellular recordings. As many as six or seven "paired" extracellular and intracellular signals were seen for a single track as the intracellular electrode impaled either dendrites or somata as it was advanced through the s. oriens, s. pyramidale, and s. radiatum (~90% of all intracellular electrode tracks yielded some simultaneous activity on the intracellular and extracellular electrodes). Of the numerous attempts to obtain stable intracellular recordings from cells also recorded by the tetrode, we were able to obtain recordings from 33 neurons. With practice, >75% of intracellular electrode tracks passed through the recordable volume of the extracellular tetrode. A subset of 22 neurons were selected for further analysis because they had stable intracellular recordings with resting potentials more negative than -55 mV as well as satisfactory anatomical labeling. This subset consisted of 21 pyramidal cells and one interneuron, all of which were morphologically identified by staining for the intracellularly injected biocytin. The track of the extracellular tetrode was
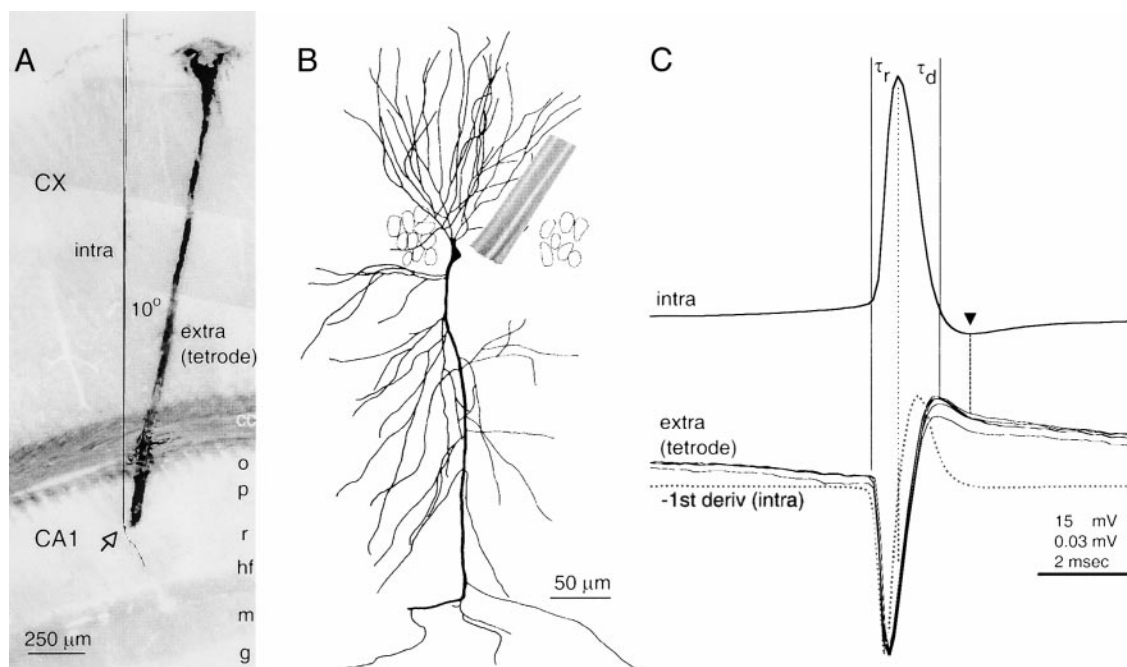
FIG. 1. Simultaneous intracellular and extracellular recording from a CA1 pyramidal cell. *A*: montage of the dorsal hippocampal area CA1 and overlying cortex showing the placement of electrodes from a successful simultaneous recording. The tetrode tip was placed in the CA1 pyramidal layer. A sharp glass pipette was then lowered into the vicinity of the tetrode tip and a CA1 pyramidal cell was impaled (↑). The path of the extracellular electrode is marked by blood on withdrawal of the tetrode. The intracellular pipette is added schematically based on the known 10° angle between the electrodes and on the location of the biocytin-labeled cell (↑). cc, corpus collosum; o, stratum oriens; p, pyramidal layer; r, stratum radiatum; hf hippocampal fissure; m, dentate molecular layer; g, dentate granular layer. *B*: camera lucida reconstruction of the intracellularly labeled cell. The tetrode tip has been added drawn and placed to scale. *C*: average (*n* = 849 spikes) intracellular action potential (intra) and extracellular spike (wideband, 1 Hz to 3 kHz, extra) recorded from the neuron (↑) in *A* and *B*. τ_r and τ_d indicate the rising and falling phases respectively of the intracellular action potential. The negative of the first derivative (1st deriv; · · ·) of the intracellular action potential is superimposed on the four traces from the extracellular tetrode. Note the relatively good match of the derivative to the tetrode traces on the initial negative phase and mismatch on the later phases of the extracellular spike. ▼, the point of slope change in the late positive phase of the extracellular spike. This cell is identified as *D53* in Fig. 6*A*.

reconstructed from the extracellular blood cells present after the tetrode was withdrawn. Figure 1, *A* and *B*, illustrates the arrangement of the recording electrodes with respect to a single pyramidal cell as well as simultaneously recorded average intracellular action potentials and extracellular spikes for that cell.

Temporal relationship between extracellularly and intracellularly recorded action potentials

Figure 1*C* illustrates the main features of an average intracellularly recorded action potential and the average extracellularly recorded "spike" for the same cell illustrated in *A* and *B*. The intracellular action potential had a waveform typical of a recording obtained from the soma of CA1 pyramidal cells (Kamondi et al. 1998). The wideband filtered (1 Hz to 3 kHz) extracellular spike waveform was also typical for normal tetrode recordings consisting of an initial large negative deflection, followed by a wider and smaller positivity (Csicsvari et al. 1999a). In some cases, the average extracellular spike was preceded by a slow negativity that most likely reflected the field electroencephalographic (EEG) signal corresponding to the intracellular excitatory postsynaptic potential (EPSP) leading to the action potential. The early large negative deflection of the extracellularly recorded spike corresponded in time to the depolarizing phase of the action potential. The later posi-

tive deflection of the extracellular spike corresponded to the depolarizing and afterhyperpolarization phases of the intracellular action potential.

We quantified the temporal relationship between the extracellular and intracellular waveforms for three "fixed" time points: the start time, the "peak" time, and the "end" time (the
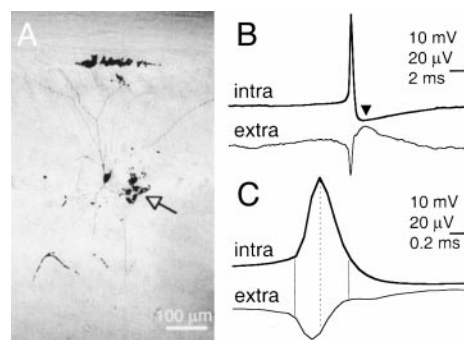

FIG. 2. Simultaneous intracellular and extracellular recording from a CA1 basket cell. *A*: micrograph of the dorsal hippocampal area CA1 showing a basket cell recorded simultaneously with intracellular and extracellular electrodes. Numerous labeled boutons were found in the CA1 pyramidal layer (not shown). ←, the location of the tip of the extracellular tetrode. *B*: average intracellular action potential of the basket cell (intra) and simultaneously recorded extracellular spike. *C*: same traces as in *B* but on an expanded time base to illustrate the relationship between the intracellular and extracellular traces. Note the short-duration and fast spike repolarization of the basket neuron.
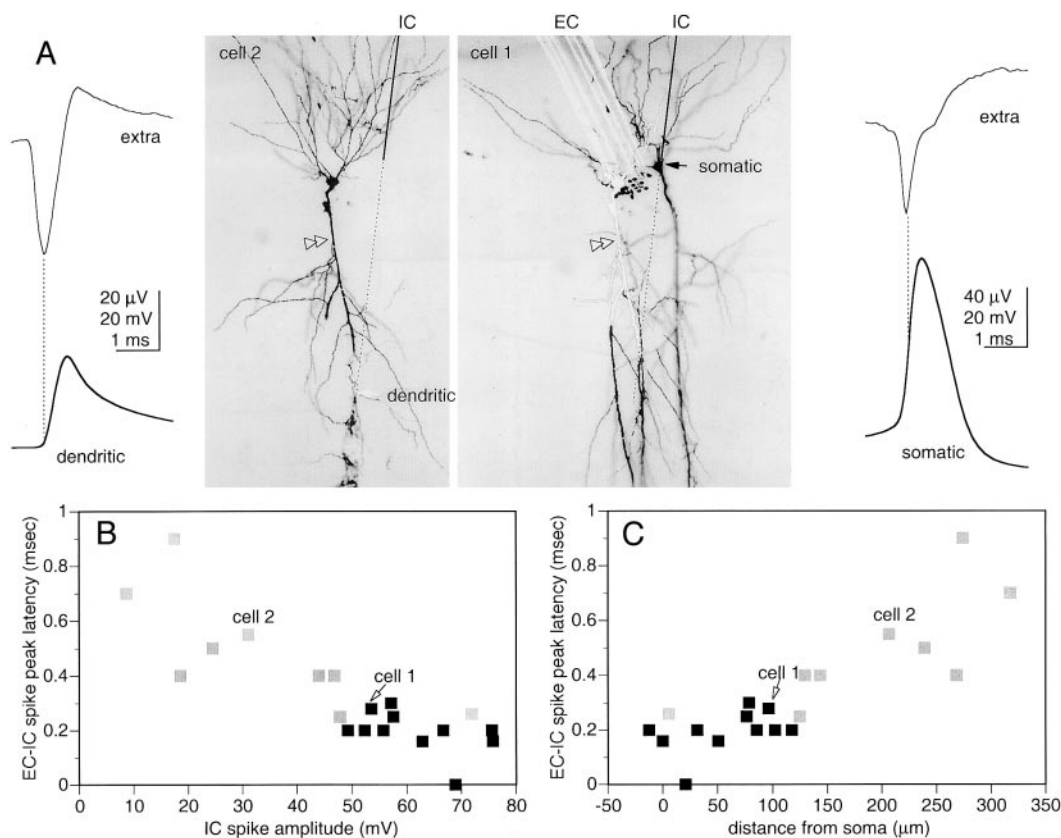
FIG. 3. Somato-dendritic intracellular recording site influences temporal relationship between extracellular and intracellular recordings. *A*: 2 simultaneous recordings from CA1 pyramidal cells recorded separately using the same intracellular electrode. *Cell 1* was recorded first from its soma (black arrow) and *cell 2* was recorded afterwards from its dendrite (white arrow). The cell bodies of the 2 cells were found in consecutive 60-μm sections (*left* and *right*). To illustrate the spatial relationship of the neurons, the soma and proximal dendrites of *cell 2* are superimposed (in white) on the image of *cell 1*. The position of the tetrode (*right*) was inferred from the blood cells. The average intracellular and extracellular waveforms are given to the right and left of *cells 1* and *2,* respectively. Note the difference in the temporal relationship between the peak of the extracellular spike and the peak of the intracellular action potential. *B*: the measured latency of the peak of the intracellular action potential following the peak of the extracellular spike as a function of the amplitude of the intracellularly recorded action potential for all 20 pyramidal cells in the database. The black symbols indicate intrasomatic recordings and the gray symbols indicate intradendritic recordings. *C*: the same data presented in *B* replotted using the data of Kamondi et al. (1998) to estimate the distance of the intracellular recording site based on intracellular action potential amplitude. Symbols as in *B*.

return to threshold potential for intracellular, and the peak of the late positivity for the extracellular). For the 11 somatic intracellular recordings obtained for this study, the average extracellular spike started 0.01 ± 0.02 (SD) ms and ended 0.02 ± 0.14 ms earlier than the corresponding points on the average intracellular action potential. The action potential duration was calculated to be 1.28 ± 0.18 ms and 1.27 ± 0.19 ms from the intracellular and extracellular waveforms, respectively. As expected, there was a linear relationship between the intracellular and extracellular spike durations across individual cells ($R = 0.66$, $P < 0.03$). Thus the duration of the intracellular action potential (from onset to return to baseline; $\tau_r + \tau_d$ in Fig. 1*C*) is well approximated by the time elapsed between the onset and the late positive peak of the extracellularly recorded waveform. The negative peak of the extracellular spike preceded the peak of the intracellular somatic action potential by 0.20 ± 0.08 ms (ordinate values for black squares in Fig. 3, *B* and *C*).

Other relationships between the extracellular and intracellular waveforms were also observed. In some cases, following the extracellular negative peak, the ascending component of

the spike exhibited an initial fast slope followed by a period of a slower slope (e.g., Fig. 4*B*, arrow) (see also Csicsvari et al. 1999a). This "notch" on the ascending phase corresponded in time to the peak of the intracellularly recorded action potential. Following the positive peak, the extracellular spike gradually returned to the baseline. Often the late positive peak was followed by a clearly recognizable change in the slope (Figs. 1*C* and 2*B*, ▼), corresponding to the peak of the intracellular spike afterhyperpolarization.

It has been proposed that the extracellular spike should be shaped like the first derivative (with respect to time) of the intracellular voltage (Brooks and Eccles 1947; Fatt 1957; Freygang and Frank 1959; Terzuolo and Araki 1961; but see Rall and Shepherd 1968). However, we have observed consistent departures from this simple model. Whereas the waveforms were similar during the ascending phase of the action potential (τ_r), they differed substantially during the descending phase and spike afterhyperpolarization (τ_d; Fig. 1*C*). We consistently observed that after the initial ascending phase (τ_r), the intracellular derivative followed a much faster trajectory than the extracellular spike.
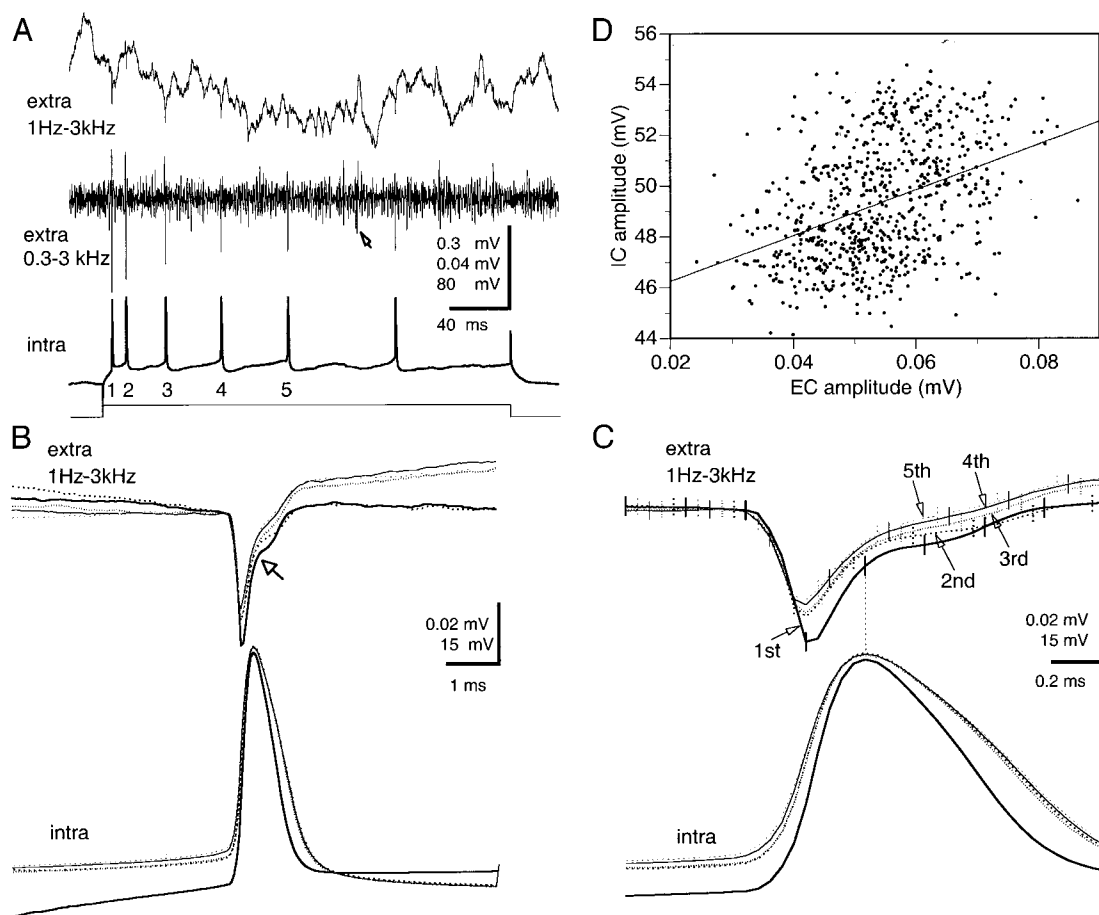
FIG. 4.   Correlated changes between the amplitude and shape of intracellular action potentials and extracellular spikes from CA1 pyramidal cells. *A*: current injection-induced (0.6 nA) action potential burst. *Top*: wideband extracellular trace (extra, 1 Hz to 3 kHz). *Middle*: highpass filtered extracellular trace (extra, 0.3–3 kHz). ↑, spike from another nearby cell. *Bottom*: intracellular trace showing action potentials evoked by the 350-ms depolarizing step (indicated below by step). *B*: extracellular (1 Hz to 3 kHz, extra) and intracellular and averages of the 1st–5th action potentials of the current step-induced trains from the cell shown in *A* (n = 243, 241, 240, 239, 176 for 1st–5th action potentials, respectively). Note progressively decreasing amplitude and increasing duration of the intracellular action potential and corresponding amplitude and shape changes of the extracellular traces. *C*: same traces as in *B* but on an expanded time base. The action potential number in the burst is indicated (→) on the extracellular traces. The vertical lines on the extracellular traces indicate the standard error of the averages. The relationship between the late notable inflection on the extracellular spike and the peak of the intracellular action potential is indicated by the dotted vertical line. *D*: the relationship between the amplitude of the intracellular action potential and the extracellular spike from a different cell where short bursts where evoked with strong depolarizing steps. The average firing frequency during the burst was ~200 Hz. —, the best fit regression line (R = 0.40; P < 0.0001).

It is important to note that the temporal relationships described above are for a wideband filtered (1 Hz to 3 kHz) extracellular waveform. Extracellular waveforms that have been filtered for higher frequencies will exhibit different relationships that will be dependent on the filter properties. Therefore we report only the relationship between the intracellular waveform and the wideband extracellular waveforms to permit comparison of data across laboratories that may use very different filters.

One additional cell was not included in the group analysis described in the preceding text. This cell was excluded based on the observation that it had an atypical extracellular waveform consisting of a large initial positivity. In this case, the tetrode appeared to have been closest to the cell body of all cells investigated. In fact, the exact relationship between the neuron and tetrode could not be determined because the red blood cell clot at the end of the extracellular tetrode track largely obscured the soma of the biocytin filled pyramidal cell.

In an additional five cases, simultaneous intracellular and extracellular recordings of action potentials were achieved with a 60-μm single wire. The qualitative findings were the same as described for tetrode recordings.

Figure 2 illustrates the relationship between the extracellular and intracellular waveforms for a basket interneuron. Although the shape of the action potential is different from pyramidal cells, the qualitative relationship between the intracellular and extracellular waveforms was the same as described in the preceding text.

Nine other pyramidal cell recordings were obtained with dendritic intracellular impalements. The recordings were determined to be from the dendrites based on the lack of a fast afterhyperpolarization and/or an action potential peak value <0 mV (Kamondi et al. 1998). The simultaneously recorded extracellular signals reflected the occurrence of the somatic action potential since the tetrode was always placed in the pyramidal layer. Figure 3*A* shows an example where
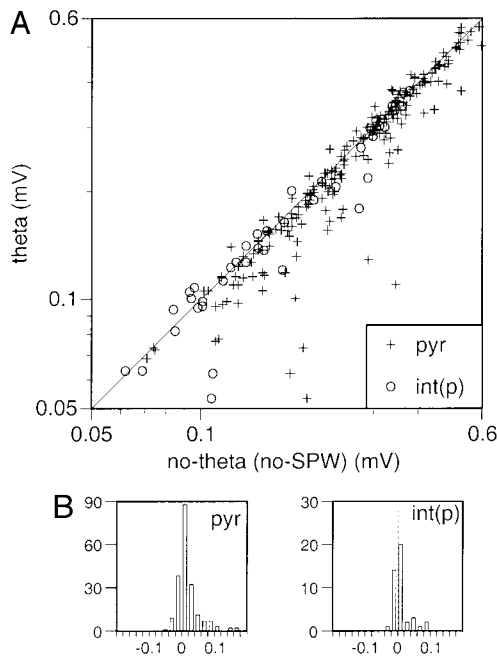
FIG. 5. State-dependent changes of extracellular spike amplitude. *A*: comparison of spike amplitudes of individual pyramidal cells ($n = 202$) and pyramidal layer interneurons [int(p)] ($n = 43$) during slow-wave sleep (no-SPW) and rapid eye movement sleep (theta) epochs. Sharp-wave bursts were excluded from this analysis. *B*: frequency histograms, derived from the *x-y* differences of the data points in *A,* show the difference between the respective states. The amplitudes of the spikes are significantly different between these 2 states; $P < 0.001$ for pyramidal cells and $P < 0.003$ for int(p). paired Student's *t*-test.

sequential recordings were obtained from two cells. The first recording was a somatic impalement that was later followed by a dendritic impalement of a different neuron 240 μm deeper. For the dendritic recording, the peak of the extracellular spike occurred 0.55 ms before the intracellular peak, whereas for the somatic recording, the extracellular spike occurred 0.28 ms before the intracellular peak. We have previously reported that the amplitude of the intracellularly recorded action potential varies directly as a function distance from the soma (Kamondi et al. 1998). Figure 3*B* shows that the latency between the extracellular peak and intracellular peak for all 21 pyramidal cells also varies as a function of intracellular action potential amplitude. If we assume that the distance between the intracellular electrode tip and the soma is the main reason for the variation in the average intracellular action potential amplitude, then we can use the relationship we have previously reported (4.9 μm/mV) (Kamondi et al. 1998) to estimate the relationship between extracellular-intracellular peak latency and intracellular recording distance from the soma (Fig. 3*C*). These data support the conclusion that under our conditions, the average action potential is initiated at the soma and back-propagates into the dendrites. The average conduction velocity of the back-propagating spike calculated from these data are 1.61 m/s.

Correlated variations in amplitude and shape between intracellular and extracellular spikes

We also investigated whether there is a correlation between changes in intracellular and extracellular spike am-

plitude and shape. We examined the relationship between the intracellular and extracellular signals during bursts of action potentials evoked by intracellular current injection (Fig. 4). Intracellular depolarizing current steps induced an accommodating series of action potentials. Figure 4, *A–C,* shows the relationships during slow evoked burst activity (1st interspike interval ∼10 ms). As expected for current-induced bursts, the intracellular waveform of the first action potential differed from subsequent action potentials. Over the course of the evoked depolarization, the amplitude of the action potential became smaller, and the slope of both the rising and falling phases decreased (lower traces in Fig. 4, *B*
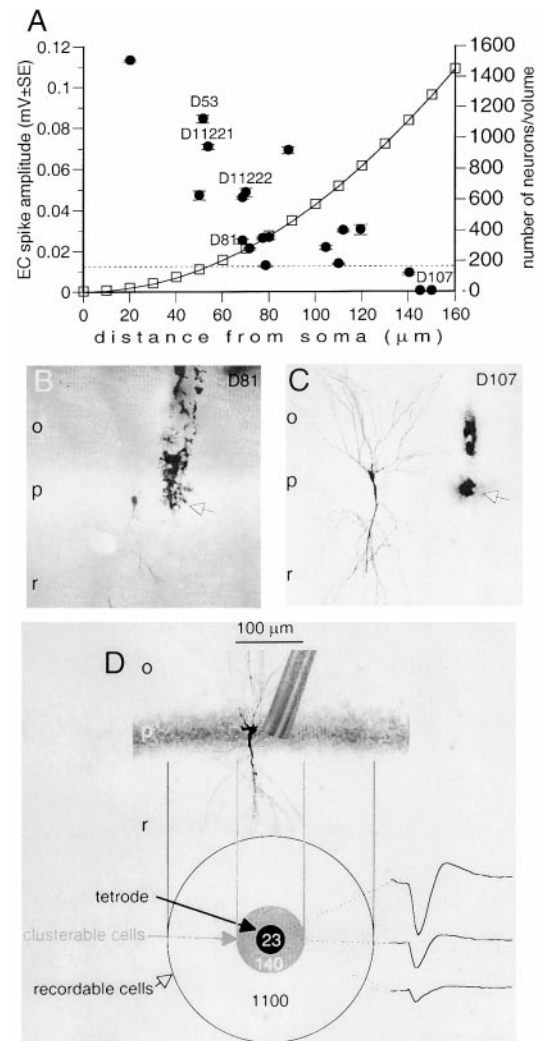

FIG. 6. Extracellular spike amplitude varies as a function of distance from the cell. *A*: left-hand ordinate and ●, average extracellular spike amplitude (± SE) vs. tetrode tip distance from 19 labeled pyramidal cells where distance estimates could be obtained. The identities of the various cells used in other figures are noted. The averages were taken from the tetrode channel with the largest peak amplitude. Right-hand ordinate and □, estimated number of neurons in the CA1 pyramidal cell layer in cylinders of increasing radius (based on data from Aika et al. 1994). *B* and *C*: examples of a relatively close and far tetrode position, respectively. The neuron in *B* was embedded for later electron microscopic examination. *D, top*: relationship of a CA1 pyramidal cell and a tetrode composed of 12.5-μm wires drawn to scale. *Bottom*: an estimate of the area and number of CA1 pyramidal cells from which a single tetrode can obtain recordings. Gray area indicates a 50-μm radius in which the amplitude of the extracellular spike exceeds 60 μV and therefore cells should be separable using current clustering methods.
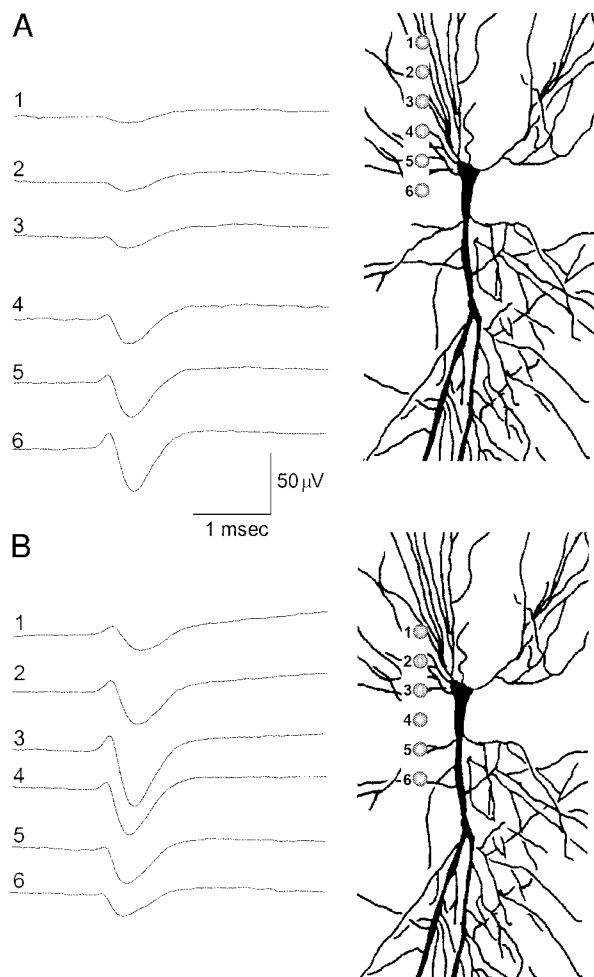
FIG. 7. Simultaneous recording of extracellular spike waveforms by a linear array of 6 electrodes (silicon "hexatrode"). The hypothesized relationship between the recording sites (1–6; 25-μm vertical spacing) and the pyramidal cell is shown on the *right*. Each trace is an averaged waveform. Channel 6 is hypothesized to be the closest to the soma. *B*: the silicon probe was moved 75 μm deeper relative to the position shown in *A*. Note that the channel with the largest spike is now channel 3, consistent with a movement of 75 μm of the electrode. Filter settings: 1 Hz to 10 kHz.

and *C*). These data also indicate that the amplitude of the somatic intracellular action potential changes due to a depolarization of the baseline membrane potential and not due to changes in the peak potential of the action potential. The observed intracellular waveform changes were accompanied by commensurate alterations of the extracellular waveforms. The amplitude of the extracellular spike decreased, the slope of the positive-going phase of the spike decreased and the "notch" became less prominent (Fig. 4, *B* and *C*). Figure 4*D* shows, for a different cell, the relationship between the extracellular spike amplitude and intracellular action potential amplitude for bursts of spikes occurring at a higher frequency (~5-ms inter-spike intervals). The best fit line ($R = 0.40$; $P < 0.0001$) illustrates the positive relationship between the intracellular and extracellular amplitudes. Taken together, these findings indicate that *relative* changes in the extracellular spike amplitude over the course of a recording session can be used to make predictions about *relative* changes in intracellular membrane potential at the time of the spike.

Behavioral state effects on extracellular spike waveform

As shown in the preceding text, depolarization exerts an effect on the amplitude and shape of the extracellular spikes (Fig. 4). We examined whether the amplitude of the extracellularly recorded spikes was affected by the state-dependent modulation of the membrane potential in nonanesthetized behaving animals. Extracellular spike amplitudes for individual units during rapid-eye movement (REM) sleep associated with theta oscillation were compared with spikes from the same units collected during slow wave sleep in the absence of theta (Fig. 5). The amplitude of individual spikes was measured from the negative to the positive peak of each waveform. Spikes during sharp wave (SPW) bursts were omitted from the analysis to avoid potential contamination from temporally overlapping spikes during population bursts associated with sharp waves (Buzsaki et al. 1983; Harris et al. 2000). This comparison revealed that the mean spike amplitude of individual pyramidal units and pyramidal layer interneuronal units was lower during theta oscillations ($P < 0.003$; paired Student's *t*-test). Based on the findings from Fig. 4, one possible explanation for the relatively smaller spike amplitudes during theta (Buzsaki et al. 1983; Csicsvari et al. 1999a) is that many of the action potentials of both pyramidal cells and pyramidal layer interneurons are initiated from more depolarized membrane potentials during theta activity. This is further supported by the fact that the frequency of discharge of both pyramidal cells and interneurons is higher during theta activity than during "no-theta and no-sharp wave" periods.

Field measurements of action potentials

The simultaneous intracellular and extracellular recordings from single neurons also allowed us to examine the spread of spikes in the extracellular space. We found that the amplitude of the average extracellular spike decreased rapidly as a function of distance of the tetrode tip from the soma. Figure 6*A* shows the amplitude of the average extracellular spike versus the distance measured between the end of the tetrode track and the intracellularly labeled cell. The largest amplitude spikes were recorded <50 μm from the soma. At distances >50 μm, individual small amplitude spikes (<60 μV) still could be recognized in the extracellular recordings at the times of the intracellular action potentials. However, the reliability of unit separation for these low-amplitude units is decreased significantly compared with spikes that are 60 μV. Under the conditions used in our laboratory, most units that can be successfully clustered are >60 μV (e.g., see lower limit of Fig. 5) (Harris et al. 2000). At extracellular distances >140 μm from the soma (Fig. 6*C*), no extracellular spike activity could be distinguished from the background noise activity even after averaging based on the occurrence of the intracellular action potentials. Unfortunately although we regularly observed extracellular spikes that were >250 μV in amplitude, we failed to obtain stable intracellular recording from such cells. We believe that this is due to the technical challenge of obtaining recordings from a very specific and small group of neurons that are very close to the tetrode tip (see Fig. 6*D*).

We have estimated the theoretical maximum number of simultaneously recordable neurons in CA1 by a single tetrode based on our measurements and an estimate of CA1 cell
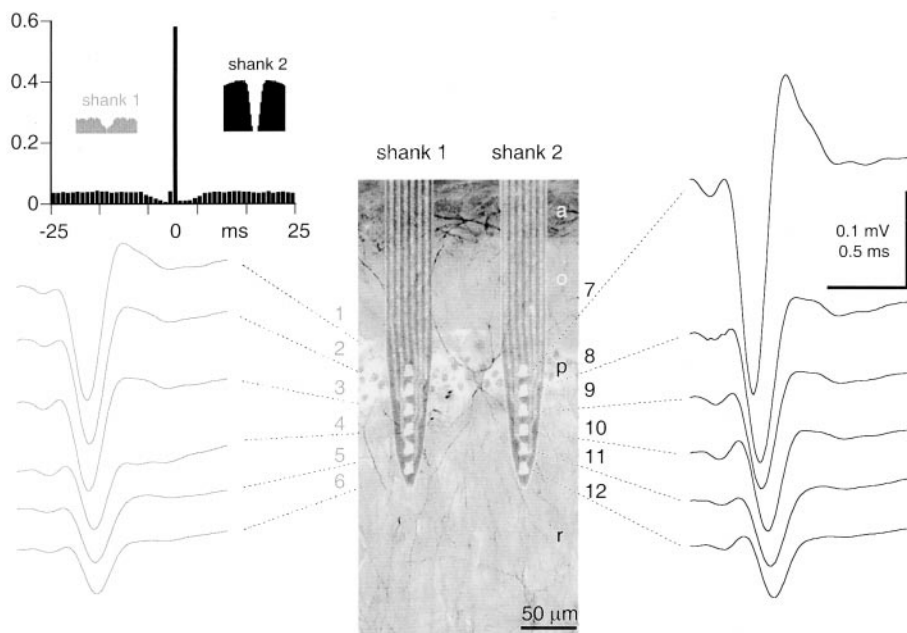
FIG. 8. Simultaneous recording from a putative pyramidal layer interneuron by 2 shanks, spaced 150 μm apart in the horizontal plane. *Middle*: hypothesized relationship between the recording sites of the 2 shanks and a calretinin-immunoreactive interneuron. Traces are wideband (1 Hz and 5 kHz) averages of >200 spikes, triggered by the spike detected in hexatrode 2 (*sites 7–12*). Unit clusters from shank 2 revealed a large amplitude interneuron and several pyramidal cells (not shown). Clusters from shank 1 revealed a poorly isolated interneuron. These features are indicated by the autocorrelograms of the respective units. Note clear refractoriness in the right autocorrelogram (shank 2) and the lack of a reliable refractory period in the left autocorrelogram (shank 1). Cross-correlogram of 2 unit clusters isolated from the 2 neighboring "hexatrodes" (shank 1 and shank 2) showed 0.6 probability of spike co-occurrence at 0 ms, flanked by suppressed spike activity (common refractoriness). Only 2 putative interneurons of all cells in our database (Csicsvari et al. 1999a) were recorded simultaneously by 2 neighboring shanks.

density of 300,000/mm^3 (Aika et al. 1994). According to our measurements (Fig. 6A), the amplitude of the spikes <50 μm from the tetrode is $\geq$60 μV and is therefore detectable and clusterable. Assuming a CA1 pyramidal layer thickness of 60 μm and a radius of 50 μm for effective cluster separation of units, a single tetrode can record >60 μV amplitude spikes from cells in a cylinder with a volume of 4.71×10^{-4} mm^3. This volume is calculated to contain 141 cells. In reality, the number of cells in this volume probably is smaller because the insertion of a tetrode (radius = 15 μm) will damage or replace $\geq$13 neurons. Finally because all cells that can be recorded from are $\leq$140 μm from the tetrode, theoretically one could record from as many as 1,108 neurons with a single tetrode with perfect recording and unit isolation methods.

Multiple recording of extracellular spikes along the somato-dendritic axis

In all of the experiments described in the preceding text, the wire tetrode was placed in the pyramidal layer and therefore the distances measured are mainly in the "lateral" direction at the level of the pyramidal cell somata. By using double-shanked silicon probes with six linearly placed recordings sites per shank (25-μm intersite distances, 150-μm intershank distance), we were also able to investigate the vertical spread of extracellular spikes perpendicular to the pyramidal layer. Figure 7 shows such a recording. The extracellular waveforms were averaged based on the occurrence of the simultaneously recorded intracellular action potentials. The extracellular channel with the largest amplitude spike was regarded as the putative location of the soma in the dorsoventral axis. Depending on the relative position of the silicon probe, extracellular units could be recorded from $\geq$100 μm above and below the putative location of the soma (Fig. 7). In other recordings from behaving animals using silicon tetrodes with 50-μm vertical separation, spikes were often simultaneously present at all four recordings sites (data not shown). Therefore we conclude that spike activity can be monitored at least over a 200-μm vertical span.

Coincident with the extracellular spike amplitude decrease, the rise and decay slopes of the extracellular spike also decreased with distance from the soma (Fig. 7). These changes in spike shape paralleled the action potential changes recorded in dendrites at various distances from the soma (Kamondi et al. 1998), although quantitative comparisons from simultaneously recorded intradendritic and extradendritic measurement are not available. The propagation velocity of action potentials, estimated from the distance of the recording sites and the delay between the negative peaks of the extracellular spikes, varied from 0.4 to 2 m/s in pyramidal cells (n = 25) and from 0.5 to 1.5 m/s in pyramidal layer interneurons (n = 6). These numbers agree with the value calculated (1.61 m/s) from the simultaneous intracellular and extracellular recordings presented in the preceding text.

A second feature of the multishank silicon probe electrodes is that they have a fixed horizontal spacing (150 or 300 μm between the shanks). Using these electrodes, we found only two cases in our database from behaving animals (<0.5% of all clustered units) (Csicsvari et al. 1999a) when the extracellular spike, recorded at one shank, was also recorded by the neighboring shank (Fig. 8). The co-occurrence of the same spike was indicated by the cross-correlogram between units clustered separately for each shank. In both cases, a large peak was present in the cross-correlogram at 0 ms, surrounded by suppressed probability of spikes within 5 ms. In other words, the cross-correlogram of these independently clustered units resembled their individual autocorrelograms. Both units were classified as putative interneurons, located in s. oriens and in the pyramidal layer. Because similar results were never observed for units that were judged to be pyramidal cells, this suggests that the action potential-associated extracellular current spread for pyramidal cells is substantially larger in the vertical than in the horizontal direction. This is to be expected for pyramidal neurons which have an open field (Hubbard et al. 1969). Furthermore we assume that our success of recording some interneurons with neighboring shanks can be explained

by the oblique or horizontal main dendrites these neurons possess (Freund and Buzsaki 1996).

DISCUSSION

The main findings of this study are that the extracellularly recorded spike reveals information about the shape of the intracellular action potential and membrane polarization and that a single tetrode placed in the CA1 pyramidal layer should theoretically be able to simultaneously record from ~100 neurons.

Relationship between intracellular action potentials and extracellular spikes

Investigating the rules that underlie neural representation requires simultaneous monitoring of a large number of cells in a behaving animal. In addition, a complete understanding requires a knowledge of the intracellular membrane potential changes that regulate the neuronal activity. The technical difficulty of obtaining multiple simultaneous intracellular recordings in an awake rat explains why traditionally these two types of information have been gathered separately by recording extracellularly or intracellularly depending on the desired information. Because the circuitry of transmembrane currents of neurons is completed via the extracellular space, these currents can be measured by electrodes placed outside the cell. The large extracellular negative wave represents the net inward currents that flow during the depolarizing portion of the intracellular action potential. In turn, the extracellular late positive wave represents the net outward currents during the repolarization and afterhyperpolarization of the intracellular action potential.

Our observations suggest that the fine temporal structure of the extracellular spike contains additional information about the intracellular action potential. Previous investigators have suggested that the extracellular unit waveform resembles the first derivative of the intracellular action potential due to the simple resistive and capacitive properties of the cell membrane (Brooks and Eccles 1947; Fatt 1957; Freygang and Frank 1959; Terzuolo and Araki 1961). Indeed the shape of the extracellular initial negative deflection can be approximated by the first derivative of the intracellular action potential. However, the late positive component of the extracellular spike is slower than is expected from the intracellular first derivative. The primary reason for this discrepancy is the fact that the extracellular spike arises due to the sum of the "leak" current, all active ionic currents and the capacitive current (Hodgkin and Huxley 1952). Only the capacitive current is proportional to the intracellular first derivative. For a small two compartment model, the derivative of the intracellular voltage and the sum of all currents across the membranes are equal (Freygang and Frank 1959). However, previous theoretical work in the olfactory bulb and our own preliminary modeling data indicate that as the morphological complexity of a simple compartmental model is increased (i.e., more compartments are added), the relationship between the intrasomatic voltage derivative and the summed membrane currents resembles the temporally mismatched relationship observed in the real data sets (Holt and Koch 1999; Rall and Shepherd 1968; our unpublished observations). These observations suggests that the details of the

later portions of the extracellular spike are influenced by complex features including neuronal morphology and active conductance distribution. In addition, the extracellular electrode is sampling extracellular currents from multiple "compartments" of a neuron due to volume conduction in the extracellular space. However, as noted in the preceding text (see Fig. 7), we found that the location of the closest cellular "compartment" along the long axis of the neuron can drastically effect the observed extracellular spike shape.

Unfortunately, the fine temporal correlation between the intracellular and extracellular waveforms is difficult to quantify for single spikes due to the fact that there are many sources of background "noise," the worst of which is overlapping spikes from other cells (Harris et al. 2000). However, our data indicate that relative information about the analogue intracellular action potentials and membrane polarization can be inferred from averages of the extracellular spike waveforms (see following text). In addition to changes in spike amplitude, shape changes in the average intracellular action potential width correspond to shape changes in average extracellular spike shape and width. Such a relationship may be useful when investigating topics such as the modulation of potassium channels in vivo since action potential width is modulated by a variety of K^+ channels including I_A, I_D, I_{kdr}, and I_c (Storm 1990).

In addition, these data further validate previous observations that suggest that the extracellular spike width is a useful measure for the separation of pyramidal cell and interneuron spikes (Buzsaki and Eidelberg 1982; Csicsvari et al. 1999a; Fox and Ranck 1981). It is known from intracellular work that interneurons generally have narrower action potentials than pyramidal cells recorded under similar conditions (Buhl et al. 1996; Lacaille et al. 1979; McBain 1995; Scharfman 1995; Sik et al. 1995). It has been assumed that a similar relationship should hold for the extracellularly recorded spikes. The data presented here provide experimental support for this assumption.

Behavioral modulation of the extracellular waveform

Different EEG states are known to be associated with different patterns of spike activity (Buzsaki et al. 1983). When we compared the amplitude of extracellular spikes from a single unit during periods of theta oscillation and nontheta/no-SPW epochs, we found that there was a significant difference in the average spike amplitude between these two states. The extracellular spike amplitudes of both pyramidal cells and interneurons in the pyramidal layer were smaller during theta activity than observed during epochs when theta oscillations were not present. Since we have also shown that the amplitude of extracellular spikes varies as a function of membrane polarization, we conclude that one possible explanation for the extracellular spike amplitude variation observed during different EEG states may be differences in the underlying membrane polarization at the time of the spikes. Although the state-dependent effect on extracellular spike amplitude was small under the present conditions, one might expect that when pyramidal cells are strongly activated by their "place" vectors (O'Keefe and Nadel 1978; Quirk and Wilson 1999), the magnitude of the intracellular depolarization could be predicted by the amplitude decrease of the extracellular spikes.

In vivo support for backpropagating dendritic action potentials

The basic temporal relationships between the intracellularly recorded action potential and the extracellular spike also provide information about the site of action potential initiation in vivo. The temporal relationship between the peaks of the average extracellular and intracellular waveforms suggest that, on average, the action potential is initiated in the soma and then backpropagates into the dendrites. These observations do not exclude the possibility of dendritically initiated spikes during periods of strong synaptic input such as during sharp waves or epileptic activity (Golding and Spruston 1998; Kamondi et al. 1998; Turner et al. 1991). In addition, we were able to estimate the conduction velocity of the backpropagating spike (1.61 m/s) by taking advantage of the known relationship between intracellular action potential amplitude and somato-dendritic recording distance (Kamondi et al. 1998). This number agrees well with another estimate of the backpropagating action potential conduction velocity calculated from data collect using linear arrays of closely spaced recording sites along the somatic and dendritic compartments of the same neuron (0.5–2.0 m/s) (Buzsaki et al. 1996).

Sensitivity of tetrodes and spatial clustering techniques

Deciphering the behaviorally relevant computations performed by neuronal networks requires that a sufficiently large portion of neurons are monitored simultaneously in the awake animal (Buzsaki et al. 1992; Deadwyler and Hampson 1995; Skaggs et al. 1996; Wilson and McNaughton 1993). Current technology uses tetrodes to record groups of neurons near the tetrode tips whose spikes are then separated off-line by spatial clustering methods. Our simultaneous intracellular and extracellular measurements indicate that the amplitude of the extracellular spike decreases rapidly with distance from the neuron and that extracellular spikes can be revealed as far as 140 μm from the cell body. Anatomical experiments estimate that a cylinder with this radius contains ~1,100 neurons in hippocampal area CA1 (Aika et al. 1994; Boss et al. 1987). Although, in theory, all these neurons can be recorded simultaneously by a single tetrode, in practice the number of neurons that are routinely isolated as separate units is substantially smaller. With the techniques currently used in our laboratory, the amplitude threshold of easily separable unit clusters is ~60 μV (Csicsvari et al. 1999a,b; Czurko et al. 1999; Hirase et al. 1999). According to the results of this paper, neurons with amplitudes >60 μV could be recorded from a distance ≤50 μm. A cylinder with this radius should contain ~120–140 neurons. Since we observe units as large as 600 μV (e.g., Fig. 5A), the relationship between amplitude and distance must be quite steep near the electrode. In fact, this is likely to be the reason why a tetrode's closely spaced recordings surfaces show substantially different amplitudes.

The estimated number of clusterable cells in CA1 is severalfold larger than the number of routinely separated unit clusters by the presently used methods (range: 1–20 per tetrode) (Csicsvari et al. 1998, 1999a; Czurko et al. 1999; Gray et al. 1995; Harris et al. 2000; ; O'Keefe and Recce 1993; Skaggs and McNaughton 1998; Skaggs et al. 1996; Tanila et al. 1997; Wilson and McNaughton 1993). Part of the discrepancy may be due to localized damage to neurons in the area immediately surrounding the tetrode. However, at its worst, localized damage can probably only account for less than half of the "missing" units, leaving *at least* 60 separable units still intact. A more likely potential reason for the large discrepancy between theory and practice is that the great majority of pyramidal cells are silent in any given environment. Thompson and Best (1989) suggested that as many as 63% of the complex cells that they could record during anesthesia and slow-wave sleep were not active during active exploration of three different test environments. Our data suggest that the real number of "silent" or slow-discharging cells is even higher since our results are based on data collected during anesthesia or sleep.

The prevalence of silent cells is further supported by examining the ratio of pyramidal cells to interneurons detected by tetrode recordings. In general, the observed ratio of simultaneously sampled interneurons and pyramidal cells is ~1:6 (Csicsvari et al. 1999a; Czurko et al. 1999; Gothard et al. 1996; O'Keefe and Recce 1993; Shen et al. 1997; Wilson and McNaughton 1993). This ratio is five times larger than predicted on anatomical grounds for the CA1 pyramidal layer (1:33) (Aika et al. 1994). Since it is commonly believed that interneurons are active in any environment and have a much higher firing rates than pyramidal cells (cf. Freund and Buzsaki 1996), it is likely that all interneurons close to the tetrode tip are detected. Therefore the discrepancy between the physiological and anatomical estimates of interneuron to pyramidal cell ratios is best explained by a large number pyramidal cells that are within range of the tetrode but do not fire sufficient numbers of spikes during the recording period to be identified as separate cells. Note that this does not mean that these undetected cells are completely silent, only that they do not fire the hundreds of spikes necessary to identify them using clustering based methods. Another important point is that the relative silence of a large portion of pyramidal neurons favors the statistical separation of those pyramidal cells that are active. If the majority of pyramidal cells were to be simultaneously active, their separation by the extracellular spike features would be nearly impossible. This logic predicts that in other brain areas or during periods of strong activity, when the density of active neurons is high, the presently available clustering methods will provide unreliable neuron separation (Harris et al. 2000).

REFERENCES

Aika Y, Ren JQ, Kosaka K, and Kosaka T. Quantitative analysis of GABA-like-immunoreactive and parvalbumin-containing neurons in the CA1 region of the rat hippocampus using a stereological method, the disector. *Exp Brain Res* 99: 267–276, 1994.

Boss BD, Turlejski K, Stanfield BB, and Cowan WM. On the numbers of neurons in fields CA1 and CA3 of the hippocampus of Sprague-Dawley and Wistar rats. *Brain Res* 406: 280–287, 1987.

Brooks CM and Eccles JC. Electrical investigations of the monosynaptic pathway through the spinal cord. *J Neurophysiol* 10: 251–274, 1947.

Buhl EH, Szilagyi T, Halasy K, and Somogyi P. Physiological properties of anatomically identified basket and bistratified cells in the CA1 area of the rat hippocampus in vitro. *Hippocampus* 6: 294–305, 1996.

BUZSAKI G AND EIDELBERG E. Direct afferent excitation and long-term potentiation of hippocampal interneurons. *J Neurophysiol* 48: 597–607, 1982.

BUZSAKI G, HORVATH Z, URIOSTE R, HETKE J, AND WISE K. High-frequency network oscillation in the hippocampus. *Science* 256: 1025–1027, 1992.

BUZSAKI G AND KANDEL A. Somadendritic backpropagation of action potentials in cortical pyramidal cells of the awake rat. *J Neurophysiol* 79: 1587–1591, 1998.

BUZSAKI G, LEUNG LW, AND VANDERWOLF CH. Cellular bases of hippocampal EEG in the behaving rat. *Brain Res* 287: 139–171, 1983.

BUZSAKI G, PENTTONEN M, NADASDY Z, AND BRAGIN A. Pattern and inhibition-dependent invasion of pyramidal cell dendrites by fast spikes in the hippocampus in vivo. *Proc Natl Acad Sci USA* 93: 9921–9925, 1996.

CSICSVARI J, HIRASE H, CZURKO A, AND BUZSAKI G. Reliability and state dependence of pyramidal cell-interneuron synapses in the hippocampus: an ensemble approach in the behaving rat. *Neuron* 21: 179–189, 1998.

CSICSVARI J, HIRASE H, CZURKO A, MAMIYA A, AND BUZSAKI G. Oscillatory coupling of hippocampal pyramidal cells and interneurons in the behaving rat. *J Neurosci* 19: 274–287, 1999a.

CSICSVARI J, HIRASE H, CZURKO A, MAMIYA A, AND BUZSAKI G. Fast network oscillations in the hippocampal CA1 region of the behaving rat. *J Neurosci* 19: RC20, 1999b.

CZURKO A, HIRASE H, CSICSVARI J, AND BUZSAKI G. Sustained activation of hippocampal pyramidal cells by "space clamping" in a running wheel. *Eur J Neurosci* 11: 344–352, 1999.

DEADWYLER SA AND HAMPSON RE. Ensemble activity and behavior: what's the code? *Science* 270: 1316–1318, 1995.

DRAKE KL, WISE KD, FARRAYE J, ANDERSON DJ, AND BEMENT SL. Performance of planar multisite microprobes in recording extracellular single-unit intracortical activity. *IEEE Trans Biomed Eng* 35: 719–732, 1988.

FATT P. Electrical potentials occurring around a neurone during its antidromic activation. *J Neurophysiol* 20: 27–60, 1957.

FOX SE AND RANCK JBJ. Electrophysiological characteristics of hippocampal complex-spike cells and theta cells. *Exp Brain Res* 41: 399–410, 1981.

FREUND TF AND BUZSAKI G. Interneurons of the hippocampus. *Hippocampus* 6: 347–470, 1996.

FREYGANG WH AND FRANK K. Extracellular potentials from single spinal motoneurons. *J Gen Physiol* 42: 749–760, 1959.

GOLDING NL AND SPRUSTON N. Dendritic sodium spikes are variable triggers of axonal action potentials in hippocampal CA1 pyramidal neurons. *Neuron* 21: 1189–1200, 1998.

GOTHARD KM, SKAGGS WE, AND MCNAUGHTON BL. Dynamics of mismatch correction in the hippocampal ensemble code for space: interaction between path integration and environmental cues. *J Neurosci* 16: 8027–8040, 1996.

GRAY CM, MALDONADO PE, WILSON M, AND MCNAUGHTON B. Tetrodes markedly improve the reliability and yield of multiple single-unit isolation from multi-unit recordings in cat striate cortex. *J Neurosci Methods* 63: 43–54, 1995.

HARRIS KD, HENZE DA, CSICSVARI J, HIRASE H, AND BUZSAKI G. Accuracy of tetrode spike separation as determined by simultaneous intracellular and extracellular measurements. *J Neurophysiol* 84: 401–414, 2000.

HIRASE H, CZURKO A, CSICSVARI J, AND BUZSAKI G. Firing rate and theta-phase coding by hippocampal pyramidal neurons during "space clamping." *Eur J Neurosci* 11: 4373–4380, 1999.

HODGKIN AL AND HUXLEY AF. A quantitative description of membrane current and its application to conduction and excitation in nerve. *J Physiol (Lond)* 117: 500–544, 1952.

HOLT GR AND KOCH C. Electrical interactions via the extracellular potential near cell bodies. *J Comp Neurosci* 6: 169–184, 1999.

HUBBARD JI, LLINAS R, AND QUASTEL DMJ. *Electrophysiological Analysis of Synaptic Transmission.* London: Edward Arnold, 1969.

KAMONDI A, ACSADY L, AND BUZSAKI G. Dendritic spikes are enhanced by cooperative network activity in the intact hippocampus. *J Neurosci* 18: 3919–3928, 1998.

LACAILLE JC, MUELLER AL, KUNKEL DD, AND SCHWARTZKROIN PA. Local circuit interactions between oriens/alveus interneurons and CA1 pyramidal cells in hippocampal slices: electrophysiology and morphology. *J Neurosci* 7: 1979–1993, 1979.

MCBAIN CJ. Hippocampal inhibitory neuron activity in the elevated potassium model of epilepsy. *J Neurophysiol* 73: 2853–2863, 1995.

MCNAUGHTON BL, O'KEEFE J, AND BARNES CA. The stereotrode: a new technique for simultaneous isolation of several single units in the central nervous system from multiple unit records. *J Neurosci Methods* 8: 391–397, 1983.

O'KEEFE J AND NADEL L. *Hippocampus as a Cognitive Map.* Oxford: Clarendon, 1978.

O'KEEFE J AND RECCE ML. Phase relationship between hippocampal place units and the EEG theta rhythm. *Hippocampus* 3: 317–330, 1993.

QUIRK MC AND WILSON MA. Interaction between spike waveform classification and temporal sequence detection. *J Neurosci Methods* 94: 41–52, 1999.

RALL W AND SHEPHERD GM. Theoretical reconstruction of field potentials and dendrodendritic synaptic interactions in olfactory bulb. *J Neurophysiol* 31: 884–915, 1968.

RECCE M AND O'KEEFE J. The tetrode: a new technique for multiunit extracellular recording. *Soc Neurosci Abstr* 15: 1250, 1989.

SCHARFMAN HE. Electrophysiological diversity of pyramidal-shaped neurons at the granule cell layer/hilus border of the rat dentate gyrus recorded in vitro. *Hippocampus* 5: 287–305, 1995.

SHEN J, BARNES CA, MCNAUGHTON BL, SKAGGS WE, AND WEAVER KL. The effect of aging on experience-dependent plasticity of hippocampal place cells. *J Neurosci* 17: 6769–6782, 1997.

SIK A, PENTTONEN M, YLINEN A, AND BUZSAKI G. Hippocampal CA1 interneurons: an in vivo intracellular labeling study. *J Neurosci* 15: 6651–6665, 1995.

SKAGGS WE AND MCNAUGHTON BL. Spatial firing properties of hippocampal CA1 populations in an environment containing two visually identical regions. *J Neurosci* 18: 8455–8466, 1998.

SKAGGS WE, MCNAUGHTON BL, WILSON MA, AND BARNES CA. Theta phase precession in hippocampal neuronal populations and the compression of temporal sequences. *Hippocampus* 6: 149–172, 1996.

STORM JF. Potassium currents in hippocampal pyramidal cells. *Prog Brain Res* 83: 161–187, 1990.

TANILA H, SHAPIRO ML, AND EICHENBAUM H. Discordance of spatial representation in ensembles of hippocampal place cells. *Hippocampus* 7: 613–623, 1997.

TERZUOLO CA AND ARAKI T. An analysis of intra- versus extracellular potential changes associated with activity of single spinal motoneurons. *Ann NY Acad Sci* 94: 547–588, 1961.

THOMPSON LT AND BEST PJ. Place cells and silent cells in the hippocampus of freely-behaving rats. *J Neurosci* 9: 2382–2390, 1989.

TURNER RW, MEYERS DE, RICHARDSON TL, AND BARKER JL. The site for initiation of action potential discharge over the somatodendritic axis of rat hippocampal CA1 pyramidal neurons. *J Neurosci* 11: 2270–2280, 1991.

WILSON MA AND MCNAUGHTON BL. Dynamics of the hippocampal ensemble code for space. *Science* 261: 1055–1058, 1993.

YLINEN A, BRAGIN A, NADASDY Z, JANDO G, SZABO I, SIK A, AND BUZSAKI G. Sharp wave-associated high-frequency oscillation (200 Hz) in the intact hippocampus: network and intracellular mechanisms. *J Neurosci* 15: 30–46, 1995.